Structure of the Photodissociation Products of CCl_4, CBr_4, and CI_4 in Solution Studied by DFT and ab Initio Calculations

Qingyu Kong,*,† Michael Wulff,† Savo Bratos,‡ Rodolphe Vuilleumier,‡ Joonghan Kim,§ and Hyotcherl Ihee*,§

European Synchrotron Radiation Facility, Grenoble Cedex 38043, BP 220, France, Laboratoire de Physique, Théorique des Liquides, Université Pierre et Marie Curie, Case Courrier 121, 4 Place Jussieu, Paris Cedex 75252, France, and Department of Chemistry and School of Molecular Science (BK21), Korea Advanced Institute of Science and Technology (KAIST), Daejeon, 305-701, Republic of Korea

Received: May 12, 2006; In Final Form: August 1, 2006

Various molecular species that can be populated during the photoreaction of carbon tetrahalides CX_4 (X = Cl, Br, I) in the gas phase and in solution have been studied by ab initio and density functional theory (DFT) calculations. Geometries, energies, and vibrational frequencies of CX_4, CX_3, CX_2, C_2X_6, C_2X_5, C_2X_4, X_2, and the isomer X_2CX-X were calculated and transition states connecting these species were characterized. Spin−orbit DFT (SODFT) computations were also performed to include the relativistic effects, which cannot be neglected for Br and I atoms. The calculated potential energy surfaces satisfactorily describe the reactions of the photoexcited CX_4 molecules. In the gas phase, the initial C−X bond rupture in CX_4 is followed by secondary C−X breakage in the CX_3 radical, leading to CX_2 and 2X, and the formation of C_2X_6 or C_2X_4 through bimolecular recombination of the CX_3 or CX_2 radicals is favored thermodynamically. In solution, by contrast, the X_2CX-X isomer is formed via X−X binding, and two CX_3 radicals recombine nongeminately to form C_2X_6, which then dissociates into C_2X_4 and X_2 through C_2X_5. The Raman intensities and the vibrational frequencies, as well as the absorption spectra and oscillator strengths of the $Br_2CBr-Br$ isomer in the gas phase and in various solvents were computed and the calculated absorption and Raman spectra of the $Br_2CBr-Br$ isomer in various solutions are in good agreement with the experimental data. The natural population analysis indicates that the $Br_2CBr-Br$ isomer corresponds to the recently reported solvent-stabilized solvated ion pair $(CBr_3^+//Br^-)_{solv}$ in the highly polar alcohol solvent. The singlet−triplet energy separations of the CX_2 radicals in the gas phase and in solution were evaluated with high level computational methods, and the optimized geometric parameters are in good agreement with the experimental results. The geometric and energetic differences between the singlet and triplet states were explained by the electronic properties of the CX_2 radicals. C_2X_4, C_2X_5, and C_2X_6 (X = Br, I) in the gas phase and in solution were optimized at different computational levels, and the optimized geometric parameters of C_2I_4 are in very good agreement with the experimental data.

1. Introduction

Carbon tetrahalides, which validate the primary tenet of the natural tetravalence of carbon,[1] have been a subject of intense studies for decades.[2−8] They have been found in the natural environment and are important sources of reactive halogens that have been linked to ozone depletion in both the troposphere and the stratosphere.[9−12] Their photochemistry in the gas and condensed phases is important for describing reactions in natural environment and has become an area of active investigation.[13−17] In early decades, the majority of research has been devoted almost exclusively to the photolysis and reactions of CCl_4. Studies using radiolysis of CCl_4 in methyl cyclohexane at low temperatures[18−20] and two-photon excitation of liquid CCl_4 at 266 nm[21] showed that the dissociation product of CCl_4 is a solvent-separated ion pair $(CCl_3^+//Cl^-)_{solv}$. Photochemistry of tetrabromomethane CBr_4 has been studied with increasing interest in recent years. However, experimental results show some discrepancies among each other. Picosecond time-resolved Raman spectroscopic study of CBr_4 in the liquid phase showed that the $Br_2CBr-Br$ isomer with a lifetime of nanoseconds is formed after UV excitation.[22] In a recent time-resolved absorption spectroscopic study, one photon excitation of CBr_4 at 266 nm in various solvents suggested formation of a solvent-stabilized solvated ion pair $(CBr_3^+//Br^-)_{solv}$.[23] The ultrafast EXAFS study on CBr_4 in cyclohexane did not show any photodissociated intermediates.[24] Due to the disagreement of the experimental data, it is of great importance to describe the photodissociation process of CBr_4 in solution with high-level quantum chemical calculations.

The carbon tetraiodide CI_4 does not show high stability in solution and the photochemistry of CI_4 in liquid phase has not been reported. Gas-phase electron diffraction study revealed that the CI_4 molecule partially decomposes during heating and the free radicals CI_2, molecules I_2 and CI_4, and small amount of C_2I_4 coexist in the gas phase.[25] Electron diffraction on thermal decomposition of CBr_4 also showed that the major decomposi-

* To whom correspondence should be addressed: E-mail: (H.I.) hyotcherl.ihee@kaist.ac.kr; (Q.K.) kong@esrf.fr.

† European Synchrotron Radiation Facility.

‡ Laboratoire de Physique, Théorique des Liquides, Université Pierre et Marie Curie.

§ Department of Chemistry and School of Molecular Science (BK21), Korea Advanced Institute of Science and Technology (KAIST).

10.1021/jp062919w CCC: $33.50
Published on Web 09/06/2006

tion products are CBr_2, with lesser amounts of C_2Br_6, CBr_3 radicals, and molecular bromine, Br_2.[26] As the major dissociation products in the gas phase, an important characteristic of the halocarbenes CX_2 is that they have two low-lying electronic states, a singlet and a triplet with markedly different geometries and chemical properties,[8] which results in their high reactivity and importance in organic reactions.

Compared to the extensive experimental investigations, there are few theoretical studies on photodissciation reaction of carbon tetrahalides.[25,27] Here, we present quantum chemical calculations to describe the whole photodissociation processes and putative photoproducts of dissociated carbon tetrahalides (CX_4, X = Cl, Br, I) in the gas phase and in solution to get a more detailed picture of the dissociation mechanism. The geometrical and electronic properties of the halocarbene radicals CX_2 and CX_3 are also evaluated with high level computations, and the results are compared with previous experimental and theoretical studies.

2. Computational Methods

Calculations were carried out by ab initio and density functional theory (DFT) methods using the Gaussian 03 code.[28] Geometries were fully optimized, and vibrational frequencies were calculated with analytical second-order derivatives. From these calculations, zero-point vibrational energies were derived and used to correct for zero-point energy (ZPE). The number of imaginary frequencies was used to characterize the nature of the structure. For the transition state, intrinsic reaction coordinate (IRC) calculations were performed to follow the reaction path. The structural parameters were also optimized with MP2 and the coupled cluster CCSD(T)[29] methods for comparison. The Becke three-parameter hybrid functional with the Lee−Yang−Parr correlation corrections (B3LYP) was used in the DFT calculation.[30,31] The all-electron basis set 6-311+G(d) for C, Cl, and Br atoms,[32] and the all-electron basis set 6-311G(d) with added d and f polarization functions and s and p diffuse functions for the I atom,[33,34] which are referred to as 6-311+G(d), were used. Calculations with the 6-311+G(3df) basis set for the $Br_2CBr-Br$ isomer and CX_2 (X = Cl, Br, I) radicals were also carried out to compare with available experimental data.

The solvent effects were calculated using self-consistent reaction field (SCRF) theory. The self-consistent isodensity polarized continuum model (SCIPCM),[35] which allows geometry optimization at the HF and DFT levels, was used to perform the solution calculation using an isodensity value of 0.0004 e/au^3.

Time-dependent density functional theory (TD-DFT)[36] was used to calculate the vertical excitation energies and oscillator strengths. The TD-B3LYP method with 6-311+G(3df) basis set was used to calculate the absorption spectra of the $Br_2CBr-Br$ isomer in the gas phase and in various solutions.

Since both Br and I atoms are heavy elements, the relativistic effects are not negligible. Therefore, we have considered the relativistic effects using relativistic effective core potential (RECP). Spin−orbit DFT (SODFT) computations were performed with NWChem program.[37] The B3LYP hybrid function with CRENBL RECP basis set for Br[38] and I atoms,[39] and all electron basis set 6-311+G(3df) for C atom were used for SODFT calculations. The valence electrons of Br and I atoms are described by modified basis sets, which are shown in Table 1S of the Supporting Information. Geometries were fully optimized including the SO effect, and vibrational frequencies were calculated.

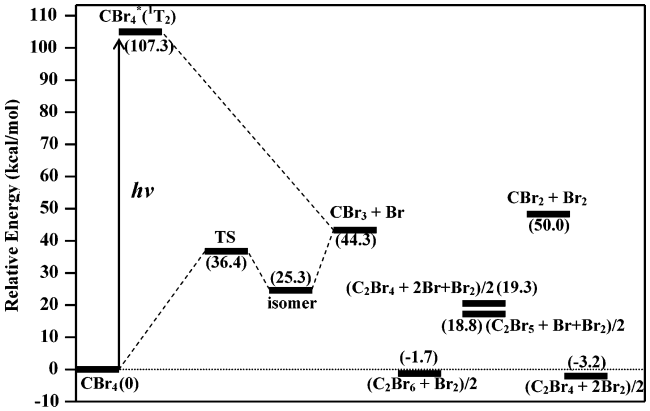

Figure 1. Potential energy levels relevant to photodissociation of CBr_4 in methanol, plotted using energies calculated at the B3LYP level with the 6-311+G(d) basis set for C and Br. The SCIPCM model is used to include the solvent effect. All energies were subjected to ZPE correction.

TABLE 1: Relative Energies (kcal/mol) of the Reaction Intermediates, Transition State, and Products in the Gas Phase and in Solution at B3LYP Level with Values in Parentheses Showing the Relative Energies from SODFT Calculations Including the Relativistic Effects[a]

		in methanol		in cyclo-
species	gas phase	6-311+G(d)	6-311+G(3df)	hexane
CBr_4	0 (0)	0	0	0
$CBr_3 + Br$	44.6 (50.0)	44.3	45.6	44.5
$CBr_2 + Br_2$	50.8 (52.1)	50.0	49.4	50.5
$CBr_2 + 2Br$	96.4	95.0	97.5	95.9
$Br_2CBr-Br$	32.2 (30.5)	25.3	25.9	30.1
$(C_2Br_6 + Br_2)/2$	−1.6	−1.7	−1.8	−1.6
$(C_2Br_5 + Br + Br_2)/2$	19.2	18.8	19.4	19.1
$(C_2Br_4 + 2Br + Br_2)/2$	19.9	19.3	20.1	19.7
$(C_2Br_4 + 2Br_2)/2$	−2.9 (−4.9)	−3.2	−4.0	−3.0
TS	44.6	36.4	36.7	41.6

[a] All the values are corrected for the zero point energies. The relative energies of $C_2Br_6 + Br_2$, $C_2Br_5 + Br + Br_2$, and $C_2Br_4 + 2Br_2$ corresponding to CBr_4 are calculated with the following formulas: $E(C_2Br_6 + Br_2)/2 - E(CBr_4)$, $E(C_2Br_5 + Br + Br_2)/2 - E(CBr_4)$, and $E(C_2Br_4 + 2Br_2)/2 - E(CBr_4)$, respectively.

3. Results and Discussion

Most of the calculations were performed in a nonpolar solvent, cyclohexane with a dielectric constant ϵ of 2.023, and in a polar alcohol solvent, methanol with a dielectric constant ϵ of 32.63. Additional calculations in 2-propanol ($\epsilon = 20.18$), acetonitrile ($\epsilon = 36.64$), propylene carbonate ($\epsilon = 66.14$), and water ($\epsilon = 78.39$) for the $Br_2CBr-Br$ isomer and in benzene ($\epsilon = 2.247$) and chloroform ($\epsilon = 4.9$) for CI_4 decomposition were also performed. In section 3.1, the whole photodissociation potential energy surfaces and various dissociation channels of carbon tetrahalides in solution and in the gas phase are presented, and in section 3.2, the putative photoproducts and their properties are presented and discussed.

3.1. Dissociation Reaction Channels. The overall potential energy levels of various candidate species along the photoreaction pathways of CBr_4 in methanol are shown in Figure 1 and the relative energies of the reaction intermediates, transition states, and products as compared to the ground-state CBr_4 molecule in the gas phase and in solution are listed in Table 1. The corresponding potential energy levels and relative energies of various candidate species of CI_4 decomposition are shown in Figure 1S and Table 2S of the Supporting Information. For a typical photodissociation at 266 nm in solution, the ground-state CBr_4 is pumped to an excited-state CBr_4* with an energy

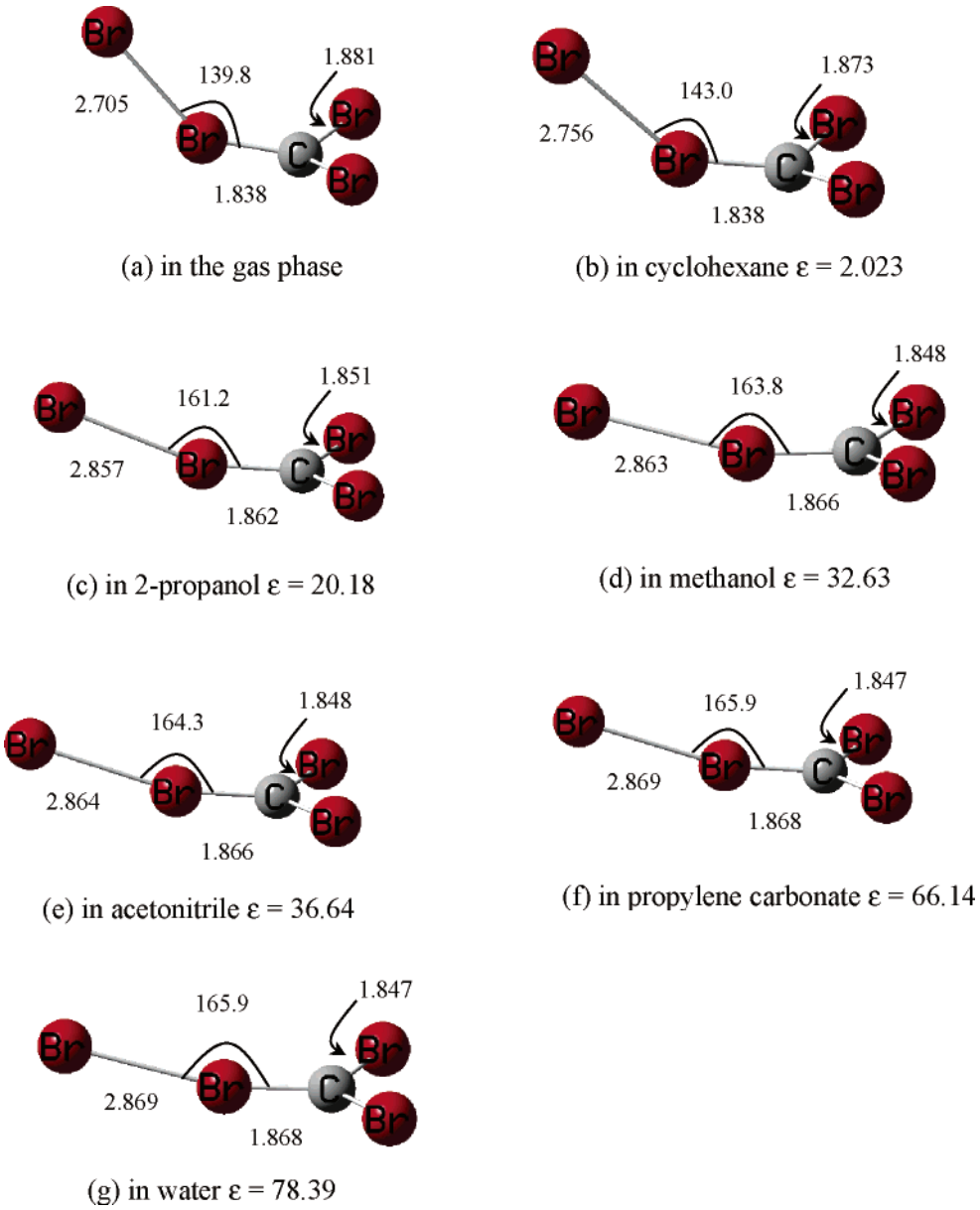

Figure 2. Geometries of the $Br_2CBr-Br$ isomer: (a) in the gas phase; (b) in cyclohexane; (c) in 2-propanol; (d) in methanol; (e) in acetonitrile; (f) in propylene carbonate; (g) in water. Calculations were performed at the B3LYP level; bond lengths are in angstroms, and angles in degrees.

of 107.3 kcal/mol (4.647 eV), which corresponds to the 12th ($^1T_2$) excited-state according to the TDDFT calculation. The first step in dissociation is to form $CBr_3 + Br$. The direct formation of $CBr_2 + 2Br$ is excluded since the laser energy at 266 nm (4.647 eV) is not sufficient to break two C−Br bonds simultaneously, which has a bond energy of 56.3 kcal/mol (2.44 eV) or 61 kcal/mol (2.64 eV) from previous experimental data.[40] The calculated C−Br bond energy is 63.1 kcal/mol (2.74 eV) in the gas phase at the MP2/6-311+G(3df) level, which basically coincides with the experimental results. The $CBr_3 + Br$ radicals, generated from the decay of the excited molecule CBr_4*, initially have an excess energy of 63.0 kcal/mol in methanol (62.8 kcal/mol in cyclohexane and 62.7 kcal/mol in the gas phase). The subsequent reactions have several pathways.

In the first case, the solvation cage may contain the liberated bromine atom within the interaction distance of the remaining bromines on CBr_3 and lead to the formation of a new species. As shown in Figure 1, the interaction of the free bromine atom with the CBr_3 radical can form a $Br_2CBr-Br$ isomer, which lies 19.0 kcal/mol lower than $CBr_3 + Br$ in methanol. The scan along the Br−Br distance of the isomer shows that there is no energy barrier for the transition from $CBr_3 + Br$ to the $Br_2CBr-Br$ isomer. The scan calculation is shown in Figure 2S of the Supporting Information. Formation of isopoly(halomethane) has been observed in the transient resonance Raman spectroscopic study of ultraviolet photoexcitation of poly(halomethane)s (CH_2Br_2, $CHBr_3$, $CFBr_3$, CBr_4, CH_2I_2, CHI_3, and CH_2IBr) in solution.[22,41] Photoexcitation of poly(halomethane)s in low-temperature matrix at 77 K also suggested isopoly(halomethane) as photoproducts.[42−47]

From our calculation, the most probable pathway following the formation of the $Br_2CBr-Br$ isomer is to relax back to the ground-state CBr_4 via a transition state. The transition state lies 11.0 kcal/mol higher than the isomer in methanol (11.5 kcal/mol in cyclohexane; 12.4 kcal/mol in the gas phase), as shown in Figure 1. Intrinsic reaction coordinate (IRC) calculations show that the transition state is a saddle point connecting the ground-state CBr_4 and the $Br_2CBr-Br$ isomer (Figure 3S in Supporting Information). The structure of the transition state in methanol is shown in Figure 4. The *XYZ* coordinates of the transition

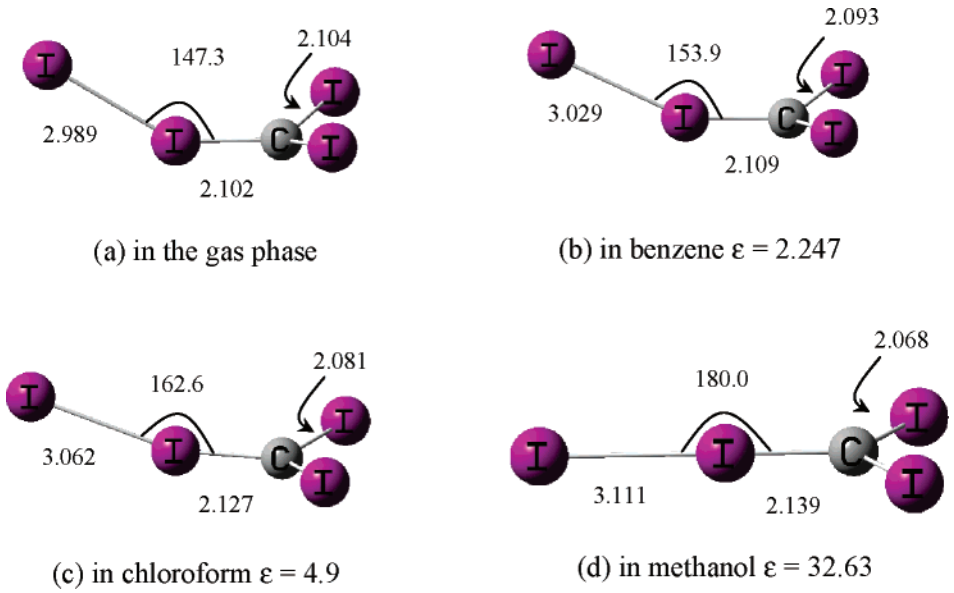

Figure 3. Geometries of the I_2CI-I isomer: (a) in the gas phase; (b) in benzene; (c) in chloroform; (d) in methanol, calculated at the B3LYP level. Bond lengths are in angstrom, and angles are in degrees. The solvent effect changes the I_2CI-I isomer from a bent structure to a linear one going from the gas phase to methanol.

states in CBr_4 and CI_4 decomposition for the gas phase and for various solvents are shown in Table 3S of the Supporting Information. The corresponding vibrational frequencies are provided in Table 4S of the Supporting Information.

Another possible reaction channel of the $Br_2CBr-Br$ isomer is to form $CBr_2 + Br_2$ through the C−Br bond breakage, which needs 24.7 kcal/mol in methanol (20.4 kcal/mol in cyclohexane, 18.6 kcal/mol in the gas phase). Compared to the relaxation reaction through the transition state, this reaction is energetically less favorable. The CX_2 (X = Br, I) radicals were not observed in the photodisscociation reaction of poly(halomethane)s in liquid[22,41] and low-temperature matrix,[42−47] indicating that the reaction to CBr_2 and Br_2 in liquid phase is not probable.

The CBr_3 and Br radicals can escape the solvation cage and interact with other partners to form C_2Br_6 and Br_2 through bimolecular recombination reactions. C_2Br_6 and Br_2 are 46.9 and 45.0 kcal/mol more stable than two free CBr_3 radicals or two free bromine atoms in methanol at B3LYP level, respectively. Energetically, C_2Br_6 or Br_2 can form directly without energy barriers as shown in Figure 1. In the gas-phase electron diffraction study on the pyrolysis of CBr_4, a well-defined peak at 4.6 Å was observed in the radial distribution function, and the data analysis indicated that the decomposition of CBr_4 resulted in about 15% conversion to C_2Br_6.[26] The dissociation reaction $C_2Br_6 \rightarrow C_2Br_4 + Br_2$ is exothermic by 2.9 kcal/mol in methanol (2.7 kcal/mol in cyclohexane, 2.6 kcal/mol in the gas phase) according to our calculation. Therefore, the C_2Br_6 molecule can decompose into C_2Br_4 and bromine. The decomposition of C_2X_6 into $C_2X_5 + X$ would be the first step involved in this process. C_2X_5 can further dissociate into $C_2X_4 + X$ or a free X can abstract another X from C_2X_5 to form $X_2 + C_2X_4$. The remaining free X atoms will eventually recombine to form X_2. In summary, the final products are $C_2X_4 + X_2$. C_2X_4 has been expected to be present as the major decomposition product of CX_4, based on thermodynamics in a previous study.[48] An electron diffraction study on pyrolysis of CI_4 in the gas phase suggested that 3% of the total diffraction intensity was from the contribution of C_2I_4.[25] From our calculations, C_2Br_4 lies 106.3 kcal/mol lower in energy than two CBr_2 radicals in methanol (107.0 kcal/mol in cyclohexane, 107.4 kcal/mol in the gas phase), indicating that C_2Br_4 can be formed directly from bimolecular combination of the CBr_2 radicals. However, since the formation of CBr_2 radicals in solution is unlikely from our calculation and previous experimental studies, C_2Br_4 in solution can be formed only through the exothermic dissociation reaction of C_2Br_6. Bimolecular combination of the CBr_2 radicals to C_2Br_4 most probably happens in the gas phase since the CX_2 (X = Br, I) radicals are the major dissociation products.[25,26] Time-resolved X-ray diffraction studies on I_2[49] and Br_2[50] in solution showed that about 10% of free iodine or bromine atoms can escape the solvation cage to undergo the nongeminate recombination reaction, indicating that the formation of C_2Br_6 and C_2Br_4 is also probable in the photodissociation reaction of CBr_4 in solution.

Pyrolysis of tetrahalides CX_4 (X = Br, I) in the gas phase showed that the CX_2 radicals are the major products. CBr_2 and CI_2 accounted for 60%[26] and 20%[25] of the final products, respectively, which indicate that the secondary dissociation of the CBr_3 radical is an important reaction channel in the gas phase. From our calculation results shown in Table 1, the secondary dissociation of the CBr_3 radical to $CBr_2 + Br$ needs an energy input of 50.7 kcal/mol in methanol (51.4 kcal/mol in cyclohexane, 51.8 kcal/mol in the gas phase). Compared to the formation of the $Br_2CBr-Br$ isomer, which does not need any energy input, the large energy barrier makes the secondary dissociation of the CBr_3 radical less probable in solution. The absence of the CBr_2 radicals in previous photodisscociation reactions in liquid [22,41] or low-temperature matrix[42−47] also confirms that the secondary dissociation of CBr_3 is not a major reaction pathway in solution even though it is so in the gas phase.

In conclusion, our calculation shows that the formation of the X_2CX-X isomer is energetically more favored than the secondary dissociation to $CX_2 + 2X$ both in the gas phase and in solution. Previous experimental results show that the isomer is the major product in solution[18−22,41] and in low-temperature matrix,[42−47] while the CX_2 radicals are formed in the gas phase,[25,26,51,52] indicating that the formation of isopoly(halomethane) is the reaction pathway in solution, whereas the secondary dissociation of the CX_3 (X = Br, I) radical is the main reaction channel in the gas phase. On the basis of our calculation and previous experimental results, the following

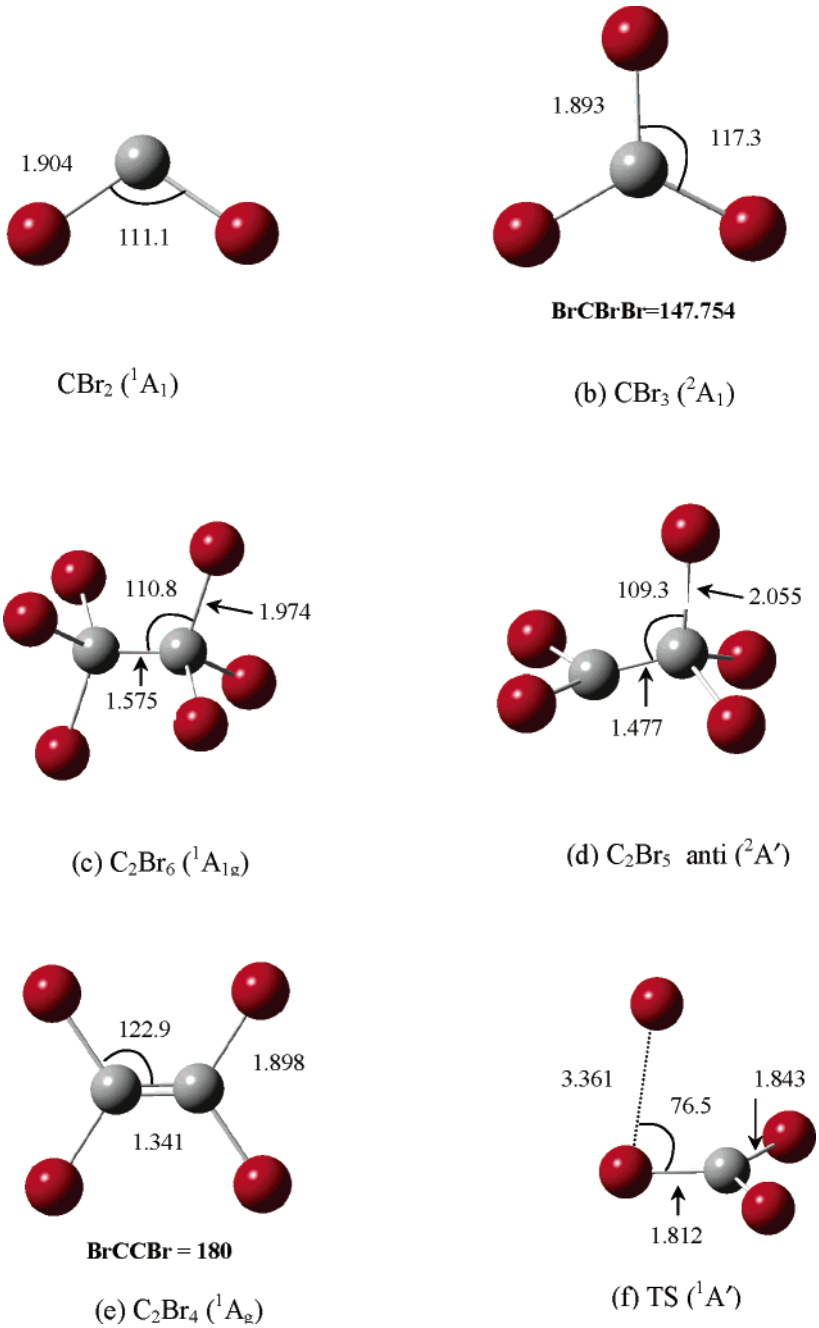

Figure 4. Geometries of (a) CBr_2 ($^1A_1$), CBr_3 ($^2A_1$), C_2Br_6 ($^1A_{1g}$), C_2Br_5– anti ($^2A'$), C_2Br_4 (^1A_g), and the transition state (TS) connecting the $Br_2CBr-Br$ isomer and ground-state CBr_4. Selected geometric parameters in methanol at B3LYP/6-311+G(d) level are shown; bond lengths are in angstroms, and angles are in degrees. Br−C−Br−Br and Br−C−C−Br indicate the dihedral angles. The SCIPCM model is used for solution calculation.

reaction mechanism of the photodissociation of carbon tetrahalides CX_4 (X = Br, I) are plausible.

In the gas phase:

$$CX_4^* \longrightarrow CX_3 + X \longrightarrow CX_2 + 2X \longrightarrow C_2X_4 + X_2$$
$$\hookrightarrow C_2X_6 + X_2 \longrightarrow C_2X_5 + X + X_2 \cdots\cdots\rightarrow C_2X_4 + 2X_2$$

In solution:

$$CX_4^* \longrightarrow CX_3 + X \longrightarrow X_2CX\text{-}X \longrightarrow TS \longrightarrow CX_4$$
$$\hookrightarrow C_2X_6 + X_2 \longrightarrow C_2X_5 + X + X_2 \cdots\cdots\rightarrow C_2X_4 + 2X_2$$

In a typical gas-phase experiment, it is less probable that the free halogen atoms encounter the CX_3 radical and have a chance to form the isomer even though the formation of the isomer is energetically more probable. As a consequence, the secondary dissociation of the CX_3 radical thus becomes the major reaction channel in the gas phase. By contrast, the solvation cage built around the solute molecules in liquid phase increases the interaction between the liberated halogen atom and the CX_3 radical. This solvation effect thus promotes the interaction between CX_3 and X to subsequently form the X_2CX-X isomer. The change of reaction pathways in going from the gas phase to solution has been established by our recent experimental and theoretical studies on the photodissociation of 1,2-diiodoethane.[53,54]

According to the above discussion, the CX_3 and X radicals, X_2CX-X isomer, and the CX_4 molecule would coexist in the photodissociation reaction of CX_4 (X = Br, I) in solution at

TABLE 2: Comparison of Calculated Vibrational Frequencies (cm^{-1}) and Raman Intensities (in Parentheses) of the $Br_2CBr-Br$ Isomer in Various Solvents at B3LYP/6-311+G(3df) Level to Previous Transient Raman Spectroscopic Experimental Data (Refs 22 and 55), Where the SCIPCM Model Was Used to Include the Solvent Effect[a]

		calculation in cyclohexane	experiment in cyclohexane	calculation in water	calculation in acetonitrile	experiment in acetonitrile and trace of water
C−Br str	A′	818.4 (58)	828	797.0 (8)	795.6 (10)	828
Br−C−Br wag	A″	761.8 (6)		775.2 (130)	777.2 (110)	
Br_2−C−Br wag	A′	343.9 (2)		411.1 (172)	408.4 (156)	
Br_2−C−Br sym Str.	A′	283.0 (7)		278.5 (334)	278.7 (289)	280
Br_2−C−Br bend	A″	181.5 (2)		185.2 (5)	185.0 (5)	
BrCBr bend + Br−Br str	A′	174.6 (14)	179	170.0 (34)	170.0 (23)	
Br−Br str. + BrCBr bend	A′	147.4 (24)	155	107.5 (13)	108.7 (23)	
torsion	A″	49.6 (5)		47.7 (14)	47.6 (15)	
$Br_2CBr-Br$ bend	A′	35.6 (10)		18.7 (28)	19.9 (23)	

[a] The Raman intensities in solution were calculated with the PCM model, based on the geometries optimized with the SCIPCM model. The SCIPCM model is not available for the Raman intensity calculation in solution.

early time delays. The CX_3 and X radicals are probably able to dimerize to form C_2X_6 and X_2, respectively, and then C_2X_6 will decompose into C_2X_4 and X_2 at late time delays. So the final products, based on thermodynamics, would be the CX_4, C_2X_4, and X_2 molecules. Compared to the DFT results, the SODFT computations give slightly different energies as shown in Table 1, but the dissociation PES dose not change.

3.2. Putative Photoproducts. *The X_2CX-X Isomer.* Figure 2 shows the structures of the $Br_2CBr-Br$ isomer in the gas phase and in various solvents. The *XYZ* coordinates of the $Br_2CBr-Br$ isomer for the gas phase and for various solvents are shown in Table 5S of the Supporting Information and the calculated vibrational frequencies are listed in Table 6S. The structure of the $Br_2CBr-Br$ isomer changes dramatically from the gas phase to solution, as shown in Figure 2. The Br−Br distance of the isomer elongates from 2.705 to 2.756 Å in going from the gas phase to cyclohexane with a dielectric constant of 2.023 and keeps increasing to 2.869 Å in water with a dielectric constant of 78.39. The Br−Br−C angle also increases from 139.8 to 165.9° in going from the gas phase to water, as shown in Figure 2. The Br−Br distance elongation and the Br−Br−C angle increase indicate that the solvent effect weakens the Br−Br interaction in the $Br_2CBr-Br$ isomer. Figure 3 shows the structures of the I_2CI-I isomers in the gas phase and in various solvent. The solvent has the same effects on the I_2CI-I isomer as described above, that is the polar alcohol solvent with stronger interaction with the solute molecule weakens the I−I interaction in the I_2CI-I isomer. An important difference from the $Br_2CBr-Br$ isomer is that the I_2CI-I isomer changes from a bending structure with C_s symmetry in the gas phase and in most of nonpolar solvents to a planar structure with C_{2v} symmetry in methanol. Since the CI_4 molecule is not stable in solution, there are no experimental reports about the photodissociation reaction of CI_4 in liquid phase. Our calculation shown in Figure 1S indicates that the I_2CI-I isomer would also be the major photodissociation products of CI_4 in solution at early time delays. The *XYZ* coordinates of the I_2CI-I isomer in the gas phase and in various solvents are provided in Table 7S, and the calculated vibrational frequencies and IR intensities in the gas phase and in various solvents are shown in Table 8S of the Supporting Information. The structure of the $Br_2CBr-Br$ isomer changes slightly when the relativistic effects are considered. The Br−Br bond length changes from 2.71 Å of the DFT calculation to 2.68 Å of the spin−orbital calculation, and the BrBrC angle changes from 140.0 to 142.1 degree. The *XYZ* coordinates of the X_2CX-X (X = Br, I) isomer in the gas phase from SODFT calculation are included in Table 5S and Table 7S of the Supporting Information, respectively.

Although the $Br_2CBr-Br$ isomer is the major product in the UV photolysis of CBr_4 in solution[22,53] and in a low-temperature matrix,[42] no direct information about geometrical parameters of the isomer has been obtained from the laser spectroscopic studies. To compare with the available experimental data, the Raman intensities and the vibrational frequencies, as well as the absorption spectra and oscillator strengths of the $Br_2CBr-Br$ isomer in the gas phase and in various solvents were computed. Table 2 shows the comparison of calculated vibrational frequencies of the $Br_2CBr-Br$ isomer in cyclohexane, acetonitrile, and water to those previously reported from transient resonance Raman spectroscopic experiments.[22,55] The calculated frequencies and Raman intensities in cyclohexane are in good agreement with the observed results. The calculation results shows that the C−Br stretching fundamental band is at 818.4 cm^{-1}, and the Br−C−Br bend and Br−Br stretching bands with less stronger Raman intensities are at 174.6 and 147.4 cm^{-1}. In comparison with the observed frequencies at 828, 179, and 155 cm^{-1}, an averaged empirical frequency scaling of 0.971 is needed between theory and experiment. Our calculation shows that the maximum Raman intensity of the $Br_2CBr-Br$ isomer changes from the C−Br stretching mode at 818.4 cm^{-1} in cyclohexane to the Br−Br−C−Br symmetric stretching mode at 278.5 and 278.7 cm^{-1} in water and acetonitrile. The calculated results accord with the experimental data, where the ν_3 Br−Br−C−Br symmetric stretching mode is more clearly observed in acetonitrile than in cyclohexane.[55] According to the computed Raman intensity in acetonitrile, the Br−C−Br wag band around 400 cm^{-1} should be observed in the acetonitrile experiment, but no experimental data about this vibrational mode has been reported in a previous study.[55]

In a recent photolysis study of CBr_4, the absorption spectra of an intermediate in various solvents were reported, and a solvent-stabilized solvated ion pair $(CBr_3^+//Br^-)_{solv}$ was suggested to form.[23] Table 3 shows the calculated absorption and oscillator strengths of the $Br_2CBr-Br$ isomer in the gas phase and in various solvent with the TD-DFT method and the comparison with the experimental data for the proposed ion pair. The computed absorption peaks in cyclohexane and dodecane are located at 482 and 480 nm respectively, which are almost identical to the observed absorption at 480 nm. The calculated absorption peak at 650 nm in the polar alcohol solvent acetonitrile is also in good agreement with the observed absorption at 635 nm. To explain the origin of this excellent agreement between the observed absorption peaks for the proposed ion pair and the calculated ones for the $Br_2CBr-Br$ isomer, we carried out natural population analysis (NPA) of the $Br_2CBr-Br$ isomer in the gas phase and in various solutions

TABLE 3: Calculated Absorption (nm) and Oscillator Strengths (in Parentheses) of the $Br_2CBr-Br$ Isomer at Different Excited States in the Gas Phase and in Various Solution at the TD-B3LYP/6-311+G(3df) Level, and Comparison with the Experimental Data[a]

	$Br_2CBr-Br$ isomer					
excited states	gas phase	in cyclohexane	in dodecane	In 2-propanol	in acetonitrile	in propylene carbonate
2	883 (0)	897 (0)	895 (0)	985 (0)	997 (0)	1000 (0)
3	799 (0)	823 (0)	821 (0)	936 (0)	955 (0)	962 (0)
4	719 (0.0002)	751 (0.0001)	749 (0.0001)	893 (0)	914 (0)	922 (0)
5	651 (0.0004)	685 (0.0002)	684 (0.0002)	824 (0)	845 (0.0001)	853 (0.0001)
6	**459 (0.1843)**	**482 (0.1951)**	**480 (0.1963)**	**622 (0.1211)**	**650 (0.1051)**	**663 (0.0988)**
7	417 (0)	406 (0)	406 (0)	429 (0)	434 (0)	436 (0)
8	374 (0)	388 (0)	387 (0)	340 (0.0001)	404 (0)	406 (0)
9	360 (0.0646)	365 (0.0001)	365 (0.0001)	382 (0)	381 (0)	381 (0)
10	357 (0)	354 (0)	354 (0.0524)	368 (0)	373 (0)	375 (0)
11	354 (0.0001)	354 (0.0516)	354 (0)	361 (0)	364 (0)	366 (0)
12	349 (0)	346 (0)	346 (0)	358 (0)	360 (0)	360 (0)
13	342 (0)	342 (0)	342 (0)	352 (0)	354 (0)	355 (0)
14	324 (0)	333 (0)	333 (0)	348 (0.0001)	349 (0.0001)	350 (0.0001)
15	315 (0)	326 (0)	326 (0)	347 (0.010)	347 (0.0070)	347 (0.0059)
16	310 (0.2370)	310 (0.2274)	310 (0.2274)	336 (0)	339 (0)	340 (0)
			Experimental Data (Ref 23)			
		480	480	540	635	635

[a] Some of the calculated excitation energies have negative values at the first excited state, so the absorption spectra were shown from nstates = 2.

TABLE 4: Computed Natural Population Analysis (NPA) of the $Br_2CBr-Br$ Isomer in the Gas Phase and in Various Solutions at the B3LYP/6-311+G(3df) Level, Where the SCIPCM Model Is Used to Include the Solvent Effects

	$Br_2CBr-Br$ isomer						
atoms	gas phase	in cyclohexane	in dodecane	in 2-propanol	in acetonitrile	in propylene carbonate	in water
Br	0.243 85	0.273 95	0.273 48	0.355 06	0.364 59	0.369 21	0.370 10
Br	0.243 85	0.273 95	0.273 48	0.355 06	0.364 59	0.369 21	0.370 10
C	−0.58708	−0.56717	−0.56793	−0.50387	−0.49618	−0.49293	−0.49240
Br	0.521 72	0.514 68	0.515 86	0.455 34	0.445 69	0.442 35	0.441 63
Br	−0.42233	−0.49541	−0.49490	−0.66160	−0.67870	−0.68784	−0.68943

as shown in Table 4. The NPA shows that the Br_2CBr group of the $Br_2CBr-Br$ isomer has a positive charge of 0.422 while the attached Br atom has a negative charge of −0.422, in the gas phase. This charge separation increases to ±0.495 in cyclohexane and keeps increasing in the highly polar alcohol solvent as shown in Table 4. In water ($\epsilon = 78.39$), the Br_2CBr group has a positive charge of 0.689, and the attached Br atom has a negative charge of −0.689. So, the $Br_2CBr-Br$ isomer can be approximated as a solvated ion pair ($Br_2CBr^+-Br^-$), especially in high polar alcohol solvent. On the basis of this, we suggest that the proposed solvent-stabilized solvated ion pair $(CBr_3^+//Br^-)_{solv}$ in a recent study[23] is actually the $Br_2CBr-Br$ isomer in our study.

The CX_2 and CX_3 Radicals. CX_2 are the major dissociation products in the gas phase. The electronic structure of the substituted carbenes is an interesting subject and has been intensively studied.[2,56] They have two low-lying orbitals, one with a_1 and one with b_1 symmetry. Depending on the arrangement of the electrons on these two orbitals, CX_2 have two electronic states, an $^1A_1$ singlet $(a_1)^2$ or a $^3B_1$ triplet $(a_1)(b_1)$ with markedly different geometries and chemical properties. The relative energies of these two states are important characteristics. Because of the large disagreement between computations and experiments about the singlet−triplet energy separation,[57,58] it is important to evaluate the ground state and singlet−triplet energy separation of CX_2 with high level computation methods both in the gas phase and in solution.

Table 5 shows the relative energies of the singlet and triplet states of CX_2 (X = Cl, Br, I) in the gas phase and in solution, and Table 6 shows the comparison of the ground-state geometrical parameters of CX_2 at various computational levels with the experimental data. The CX_2 has the $^1A_1$ singlet as the ground state at all computational levels in the gas phase and in solution. The relative energy ΔE_{S-T} becomes smaller going from Cl to I with decreasing ligand electronegativity as shown in Table 5. The ΔE_{S-T} is 18.1 kcal/mol for CCl_2, and drops to 14.1 and 7.1 kcal/mol for CBr_2 and CI_2 at the MP2 level. Because of the computational complexity, few calculations has been done on CI_2.[6,25] The ΔE_{S-T} for CI_2 is 7.5 kcal/mol at CCSD(T) level, which is lower than previous coupled cluster results of about 9 kcal/mol.[6,25] As shown in our previous study,[54] the all-electron basis set 6-311+G(d) for iodine atom gives much better results than the Stuttgart ECP basis sets. The calculated C_2I_4 geometrical parameters in the present study are also much better than previous results with the ECP basis sets for I atom,[6,25] as is shown in the next section. Therefore, the ΔE_{S-T} of 7.512 kcal/mol for CI_2 at CCSD(T) level with the all-electron basis set 6-311+G(d) for I atom would be more precise than previous results.[6,25] The optimized geometrical parameters in Table 6 are in good agreement with the experimental values, except for

TABLE 5: Relative Energies ΔE_{S-T} (kcal/mol) of the Singlet and Triplet States of CX_2 (X = Cl, Br, I) in the Gas Phase at Various Computational Levels and in Solution, Where the All-Electron Basis Sets 6-311+G(3df) for C and Br Atoms, and 6-311+G(d) for I Atom Were Used and the SCIPCM Model Was Used for Solution Calculations

	B3LYP				
	gas phase	in cyclohexane	in methanol	MP2	CCSD(T)
CCl_2	17.4	17.6	18.0	18.1	19.4
CBr_2	14.3	14.4	14.7	14.1	15.3
CI_2	7.0	7.2	7.4	7.1[a]	7.5[a]

[a] All the values are corrected for the zero point energies, except for CI_2 at MP2 and CCSD(T) levels.

TABLE 6: Comparison of the Geometrical Parameters of CX_2 (X = Cl, Br, I) at Various Computational Levels with the Experimental Data. The-all Electron Basis Sets 6-311+G(3df) for C and Br Atoms, and 6-311+G(d) for I Atom Were Used[a]

	B3LYP		MP2		CCSD(T)		experiment	
	r(C−X)	∠(X−C−X)	r(C−X)	∠(X−C−X)	R(C−X)	∠(X−C−X)	r(C−X)	∠(X−C−X)
CCl_2	1.722	109.9	1.699	109.9	1.718	109.6	1.7157(20)	109.2(2)[51]
	(1.673)	(128.9)	(1.665)	(127.8)	(1.675)	(128.1)		
CBr_2	1.899	110.7	1.868	110.5	1.891	110.4	1.74(3)	114.1[26]
	(1.840)	(130.1)	(1.823)	(129.3)	(1.834)	(129.7)		
CI_2	2.116	113.2	2.070	112.8	2.098	112.8	2.085(13)	112.3[25] [b]
	(2.038)	(133.8)	(2.014)	(132.9)	(2.024)	(134.2)		

[a] Bond lengths in Å and angles in degree. Values in parentheses are the geometrical parameters of triplet state. [b] The geometrical parameters of CI_2 from ref 25 are not direct experimental measurements but were assumed from computation.

CBr_2, for which the experimental data might be in error as mentioned in a previous study.[25] Compared to the experimental results in Table 6, the CCSD(T) method reproduces the experimental value most precisely. Another noticeable geometric characteristic for the CX_2 (X = Cl, Br, I) radicals is that a quite large difference of the X−C−X angle between singlet and triplet is observed in Table 6.

The trend of relative energy ΔE_{S-T} from Cl to I with decreasing ligand electronegativity has been explained in terms of molecular orbitals of CX_2 (X = F, Cl, Br, I) at singlet state in previous study,[25] and our calculations on the HOMO and LUMO of CX_2 at the MP2/6-311+G(3df) level produce similar results as shown in Figure 4S of the Supporting Information. The calculated s orbital coefficients of the C atom at HOMO (a_1) are as follows: (−0.05025, −0.08616, 0.25703, 0.38216, 0.04477) for CCl_2, (−0.04398, −0.07553, 0.22829, 0.33638, 0.25444) for CBr_2, and (0.03583, 0.06157, −0.18775, −0.27617, −0.04505) for CI_2 respectively, indicating that contribution from s orbital of the C atom decreases with decreased electronegativity of the ligands. The natural bond orbital (NBO) analysis shows that the ratios of the s character of the bonding orbital are 18.68%, 16.49%, and 16.29% for CCl_2, CBr_2, and CI_2 respectively, which also indicates that the ratio of s character of the bonding orbital decrease with decreased electronegativity of the ligands. Consequently, the energies of the HOMO (a_1) orbital increase from CCl_2 to CI_2. The calculated energies of the HOMO (a_1) orbital are −0.39795, −0.38054, and −0.34941 au for CCl_2, CBr_2 and CI_2, respectively. The LUMO (b_1) orbital has a strong antibonding characteristic consisting of a p_π orbital between the C atom and the ligands. As the electronegativity of the ligand decreases, the p contribution from the C atom decreases. Our calculated molecular orbital coefficients of the p orbital of the C atom at LUMO (b_1) are as follows: (0.20047, 0.33717, 0.45142, 0.57436) for CCl_2, (0.19791, 0.33359, 0.45187, 0.52439) for CBr_2 and (0.18848, 0.30756, 0.47719, 0.53311) for CI_2, respectively. The energy of the LUMO (b_1) orbital decreases as the p contribution of the C atom drops. The calculated energies of the LUMO (b_1) orbitals are 0.2782, 0.01376, and −0.34941 au for CCl_2, CBr_2, and CI_2. Therefore, the energies of HOMO (a_1) and LUMO (b_1) orbitals become closer as the electronegativity of the ligands decrease. Consequently, the relative energies ΔE_{S-T} of CX_2 decrease from Cl to I with decreased electronegativity.

The CX_3 radical is the major products in the first step of the dissociation reaction of CX_4 (X = Cl, Br, I). The ground-state CX_3 ($^2A_1$) has a pyramid structure in the gas phase and in solution. As an example, the geometry of CBr_3 is shown in Figure 4. The *XYZ* coordinates of CX_3 in the gas phase and in solution are shown in Table 9S of the Supporting Information, and the calculated vibrational frequencies in Table 10S. The SODFT calculation produces the same geometrical parameters for the CBr_2 and CBr_3 radicals in the gas phase, and the *XYZ* coordinates of the CBr_3 radical from SODFT calculation are included in Table 9S.

TABLE 7: Geometric Parameters of C_2Br_4, C_2Br_6, C_2I_4, and C_2I_6 Computed at the MP2 Level and Comparison with the Experimental Results of C_2I_4, Where the All-Electron Basis Sets 6-311+G(d) for C and Br Atoms and 6-311+G(d) for I Atom Were Used[a]

geometric parameters	computed				exptl data[59] of C_2I_4
	C_2Br_6	C_2Br_4	C_2I_6	C_2I_4	
r(C−C)	1.572	1.358	1.557	1.363	1.363(15)
r(C−X)	1.952	1.881	2.177	2.091	2.106(5)
∠(X−C−C)	110.5	122.4	111.4	122.9	122.9(5)

[a] Bond lengths in Å and angles in degree. The C−C, C−I bond lengths and I−C−C bond angle of C_2I_4 were calculated to be 1.347 Å, 2.084 Å and 123.3° with the ECP basis set for I atom from a previous study.[25]

C_2X_6 and C_2X_4. C_2Br_6 and C_2Br_4 are 47.0 and 106.3 kcal/mol more stable than two CBr_3 or CBr_2 radicals in methanol at B3LYP/6-311+G(d) level. Both CBr_3 and CBr_2 may dimerize. As discussed in section 3.1, C_2Br_6 probably forms through bimolecular recombination of two CB_3 radicals and dissociate to C_2Br_4 and Br_2 as the final products in solution. Formation of CBr_2 radicals is excluded from our calculation and previous experimental studies,[22,42−47] so the direct formation of C_2Br_4 through CBr_2 dimerization is not relevant in solution. The bimolecular recombination of CX_2 to C_2X_4 probably happens in the gas phase as suggested by the electron diffraction of pyrolysis of CI_4.[25] The structures of C_2Br_6 and C_2Br_4 in methanol are shown in Figure 4. The calculated *XYZ* coordinates of C_2X_6 and C_2X_4 (X = Br, I) in the gas phase and in various solutions at B3LYP level are shown in Table 11S and Table 13S of the Supporting Information, and the vibrational frequencies are shown in Table 12S and Table 14S, respectively.

Since the experimental data about C_2Br_6 from gas-phase electron diffraction study might be in error,[26] and the C_2I_6 did not form in thermal dissociation of CI_4,[25] the experimental data are available only for C_2I_4 in the gas phase.[59] Table 7 shows the geometric parameters of C_2Br_4, C_2Br_6, C_2I_4, and C_2I_6 at the MP2 level, and the comparison with the experimental data of C_2I_4. The computed C−C and C−I bond lengths of 1.363 and 2.091 Å and I−C−C bond angle of 122.9° for C_2I_4 are in very good agreement with the measured C−C and C−I bond lengths of 1.363 and 2.106 Å and the I−C−C bond angle of 122.9°.[59] Compared to the previous MP2 results with ECP basis set for I atom,[25] the present study with the all-electron basis set 6-311+G(d) for I atom gives better results. C_2X_6 have two possible structures; the staggered and eclipsed conformer. The energies of the eclipsed conformers are 23.3 and 28.8 kcal/mol higher than those of the staggered conformers for C_2Br_6 and C_2I_6 respectively at the MP2 level. The *XYZ* coordinates of the eclipsed conformers of C_2X_6 (X = Br, I) at the MP2 level are shown in the Supporting Information Table 15S.

C_2X_5. Our calculation shows that C_2Br_6 dissociates through an intermediate molecule C_2Br_5. Two conformers, the anti and bridged structures of the C_2X_5 (X = Br, I) molecule were calculated. The anti conformer of C_2Br_5 is the ground-state structure in the gas phase and in solution, while the bridged conformer has imaginary frequencies, indicating that it is a saddle point in the potential energy surface. The structure of C_2Br_5 in methanol is shown in Figure 4. C_2I_5 also has the anti conformer as the ground state, while the bridged structure has an imaginary frequency, in the gas phase. The calculated *XYZ* coordinates of C_2X_5 (X = Br, I) in the gas phase and in various solutions at B3LYP level are shown in Table 16S of the Supporting Information, and the vibrational frequencies are shown in Table 17S.

4. Conclusion

The photodissociation of CX_4 (X = Br, I) in the gas phase and in various solutions was investigated with ab initio and DFT methods. The relativistic effects were evaluated with Spin−Orbit DFT (SODFT) computations. According to our calculation, the excited CX_4* dissociates in a multistep process: in the gas phase, initial C−X bond rupture is followed by secondary cleavage of the C−X bond in the CX_3 radical. In solution, the X−X binding reaction to form the X_2CX-X (X = Br, I) isomer becomes the most important pathway and formation of C_2X_6 through nongeminate recombination of the CX_3 radicals followed by the dissociation to C_2X_4 and X_2 is a parallel reaction channel. The calculated absorption and Raman spectra of the $Br_2CBr-Br$ isomer in various solutions are in good agreement with the experimental data. The natural population analysis indicates that the $Br_2CBr-Br$ isomer corresponds to the recently reported solvent-stabilized solvated ion pair $(CBr_3^+//Br^-)_{solv}$ in the highly polar alcohol solvent. The CX_2 (X = Cl, Br, I) radicals have the $^1A_1$ singlet as the ground state in the gas phase and in solution at various computational levels. The optimized geometric parameters of C_2I_4 are in good agreement with the experimental results.

Acknowledgment. This work was supported by EU Grants FAMTO (HPRICT-1999-50004) and FLASH (FP6-503641), and by a grant from the Nano R&D Program of the Korea Science and Engineering Foundation (2005-02638) awarded to H.I.

Supporting Information Available: Tables showing the valence basis sets of Br and I atoms, which were used in the SODFT calculations, relative energies of the reaction intermediates, transition state, and products of CI_4 decomposition in the gas phase, in methanol, benzene, and chloroform at the B3LYP level, optimized structural parameters and the *XYZ* coordinates of the transition states connecting X_2CX-X isomer and CX_4 (X = Br, I) in the gas phase and in various solvents at the B3LYP level, calculated vibrational frequencies and IR intensities of the transition states (TS) connecting X_2CX-X isomer and CX_4 (X = Br, I) in the gas phase and in various solvents, optimized *XYZ* coordinates of the $Br_2CBr-Br$ isomer in the gas phase and in various solvents at the B3LYP level, calculated vibrational frequencies, IR intensities of the $Br_2CBr-Br$ isomer in the gas phase and in various solvents at B3LYP level, optimized *XYZ* coordinates of the I_2CI-I isomer in the gas phase and in various solvents at the B3LYP level, calculated vibrational frequencies and IR intensities of the I_2CI-I isomer in the gas phase and in various solvents at the B3LYP level, optimized *XYZ* coordinates of the CX_3 (X = Cl, Br, I) radicals in the gas phase and in various solvents at the B3LYP level, calculated vibrational frequencies and IR intensities of the CX_3 (X = Cl, Br, I) radicals in the gas phase and in various solvents at the B3LYP level, optimized *XYZ* coordinates of C_2X_6 (X = Br, I) in the gas phase and in various solvents at the B3LYP level, calculated vibrational frequencies, IR intensities of C_2X_6 (X = Br, I) in the gas phase and in various solvents at the B3LYP level, optimized *XYZ* coordinates of C_2X_4 (X = Br, I) in the gas phase and in various solvents at the B3LYP level, calculated vibrational frequencies and IR intensities of C_2X_4 (X = Br, I) in the gas phase and in various solvents at the B3LYP level, optimized *XYZ* coordinates of the eclipsed C_2X_6 (X = Br, I) conformers in the gas phase at the MP2 level, and optimized *XYZ* coordinates of C_2X_5 (X = Br, I) with the anti conformer in the gas phase and in various solvents at the B3LYP level, and calculated vibrational frequencies and IR intensities of C_2X_5 (X = Br, I) in the gas phase and in various solvents at the B3LYP level, and figures showing the potential energy levels of the photodissociation of CI_4 in methanol, plotted using energies calculated at the B3LYP level, 6-311+G(d) basis set for C and 6-311+G(d) basis set for I, optimized PES along the Br−Br distance of the $Br_2CBr-Br$ isomer, which indicates that no energy barrier exists between CBr_3 + Br and the $Br_2CBr-Br$ isomer, IRC calculation of the transition state connecting CBr_4 and the $Br_2CBr-Br$ isomer in the gas phase, indicating that the transition state is a saddle point connecting CBr_4 and the $Br_2CBr-Br$ isomer and HOMO and LUMO depictions of singlet ($^1A_1$) and triplet ($^3B_1$) CX_2 (X = Br, I) at the MP2 level. This material is available free of charge via the Internet at http://pubs.acs.org.

References and Notes

(1) Liebman, J. F., Greenberg, A., Eds. *Molecular Structure and Energetics*; VCH Publishers: New York, 1986; Vol. 1, p 51.
(2) Gutsev, G. L.; Ziegler, T. *J. Phys. Chem.* **1991**, *95*, 7220.
(3) Russo, N.; Sicilia, E.; Roscano, M. *J. Chem. Phys.* **1992**, *97*, 5031.
(4) Gobbi, A.; Frenking, G. *J. Chem. Soc., Chem. Commun.* **1993**, 1162.
(5) Irikura, K. K.; Goddard, W. A., III; Beauchamp, J. L. *J. Am. Chem. Soc.* **1992**, *114*, 48.
(6) Lee, E. P. F.; Dyke, J. M.; Wright, T. G. *Chem. Phys. Lett.* **2000**, *326*, 143.
(7) Hajgató, B.; Nguyen, H. M. T.; Veszprémi, T.; Nguyen, M. T. *Phys. Chem. Chem. Phys.* **2000**, *2*, 5041.
(8) Sendt, K.; Bacskay, G. B. *J. Chem. Phys.* **2000**, *112*, 2227.
(9) Molina, M. J.; Rowland, F. S. *Nature (London)* **1974**, *249*, 810.
(10) Molina, M. J.; Tso, T. L.; Molina, L. T.; Wang, F. C. Y. *Science* **1987**, *238*, 1253.
(11) McElroy, C. T.; McLinden, C. A.; McConnell, J. C. *Nature (London)* **1999**, *397*, 338.
(12) Alicke, B.; Hebestreit, K.; Stutz, J.; Platt, U. *Nature (London)* **1999**, *397*, 572.
(13) Vogt, R.; Crutzen, P. J.; Sander, R. *Nature (London)* **1996**, *383*, 327.
(14) Oum, K. W.; Lakin, M. J.; DeHaan, D. O.; Brauers, T.; Finalyson-Pitts, B. J. *Science* **1998**, *279*, 74.
(15) Knipping, E. M.; Lakin, M. J.; Foster, K. L.; Jungwirth, P.; Tobias, D. J.; Gerber, R. B.; Dabdub, D.; Finalyson-Pitts, B. J. *Science* **2000**, *288*, 301.
(16) Finalyson-Pitts, B. J.; Hemminger, J. C. *J. Phys. Chem. A* **2000**, *104*, 11463.
(17) Foster, K. L.; Plastridge, R. A.; Bottenheim, J. W.; Shepson, P. B.; Finalyson-Pitts, B.; Spicer, J. C. W. *Science* **2001**, *291*, 471.
(18) Gremlich, H. U.; Buhler, R. E. *J. Phys. Chem.* **1983**, *87*, 3267.
(19) Buhler, R. E.; Funk, W. *J. Phys. Chem.* **1978**, *79*, 2098.
(20) Buhler, R. E.; Hurni, B. *Helv. Chim. Acta* **1978**, *61*, 90.
(21) Miyasaka, H.; Masuhara, H.; Mataga, N. *Chem. Phys. Lett.* **1985**, *118*, 459.
(22) Zheng, X. M.; Fang, W. H.; Phillips, D. L. *J. Chem. Phys.* **2000**, *113*, 10934.
(23) Zhang, H.; Dvornikov, A. S.; Rentzepis, P. M. *J. Phys. Chem. A* **2005**, *109*, 5984.
(24) Oulianov, D. A.; Tomov, I. V.; Dvornikov, A. S.; Rentzepis, P. M. *PNAS* **2002**, *99*, 12556.
(25) Hargittai, M.; Schultz, G.; Schwerdtfeger, P.; Seth, M. *Struct. Chem.* **2001**, *12*, 377.

(26) Ivey, R. C.; Schulze, P. D.; Leggett, T. L.; Kohl, D. A. *J. Chem. Phys.* **1974**, *60*, 3174.
(27) Tweeten, E. D.; Petro, B. J.; Quandt, R. W. *J. Phys. Chem. A* **2003**, *107*, 19.
(28) Frisch, M. J.; Trucks, G. W.; Schlegel, H. B.; Scuseria, G. E.; Robb, M. A.; Cheeseman, J. R.; Montgomery, J. A., Jr.; Vreven, T.; Kudin, K. N.; Burant, J. C.; Millam, J. M.; Iyengar, S. S.; Tomasi, J.; Barone, V.; Mennucci, B.; Cossi, M.; Scalmani, G.; Rega, N.; Petersson, G. A.; Nakatsuji, H.; Hada, M.; Ehara, M.; Toyota, K.; Fukuda, R.; Hasegawa, J.; Ishida, M.; Nakajima, T.; Honda, Y.; Kitao, O.; Nakai, H.; Klene, M.; Li, X.; Knox, J. E.; Hratchian, H. P.; Cross, J. B.; Bakken, V.; Adamo, C.; Jaramillo, J.; Gomperts, R.; Stratmann, R. E.; Yazyev, O.; Austin, A. J.; Cammi, R.; Pomelli, C.; Ochterski, J. W.; Ayala, P. Y.; Morokuma, K.; Voth, G. A.; Salvador, P.; Dannenberg, J. J.; Zakrzewski, V. G.; Dapprich, S.; Daniels, A. D.; Strain, M. C.; Farkas, O.; Malick, D. K.; Rabuck, A. D.; Raghavachari, K.; Foresman, J. B.; Ortiz, J. V.; Cui, Q.; Baboul, A. G.; Clifford, S.; Cioslowski, J.; Stefanov, B. B.; Liu, G.; Liashenko, A.; Piskorz, P.; Komaromi, I.; Martin, R. L.; Fox, D. J.; Keith, T.; Al-Laham, M. A.; Peng, C. Y.; Nanayakkara, A.; Challacombe, M.; Gill, P. M. W.; Johnson, B.; Chen, W.; Wong, M. W.; Gonzalez, C.; Pople, J. A. *Gaussian 03*, revision C.02. Gaussian, Inc.: Wallingford, CT, 2004.
(29) Pople, J. A.; Head-Gordon, M.; Raghavachari, K. *J. Chem. Phys.* **1987**, *87*, 5968.
(30) Becke, A. D. *J. Chem. Phys.* **1993**, *98*, 5648.
(31) Lee, C.; Yang, W.; Parr, R. G. *Phys. Rev. B* **1988**, *37*, 785.
(32) Krishnan, R.; Binkley, J. S.; Seeger, R.; Pople, J. A. *J. Chem. Phys.* **1980**, *72*, 650.
(33) Stromberg, A.; Gropen, O.; Wahlgren, U. *J. Comput. Chem.* **1983**, *4*, 181.
(34) Glukhovtsev, M. N.; Pross, A. *J. Chem. Phys.* **1995**, *103*, 1878.
(35) Foresman, J. B.; Keith, T. A.; Wiberg, K. B.; Snoonian, J.; Frisch, M. J. *J. Phys. Chem.* **1996**, *100*, 16098.
(36) Stratmann, R. E.; Scuseria, G. E.; Frisch, M. J. *J. Chem. Phys.* **1998**, *109*, 8218.
(37) Aprà E.; Windus, T. L.; Straatsma, T. P.; Bylaska, E. J.; de Jong, W.; Hirata, S.; Valiev, M.; Hackler, M.; Pollack, L.; Kowalski, K.; Harrison, R.; Dupuis, M.; Smith, D. M. A.; Nieplocha, J.; Tipparaju, V.; Krishnan, M.; Auer, A. A.; Brown, E.; Cisneros, G.; Fann, G.; Fruchtl, H.; Garza, J.; Hirao, K.; Kendall, R.; Nichols, J.; Tsemekhman, K.; Wolinski, K.; Anchell, J.; Bernholdt, D.; Borowski, P.; Clark, T.; Clerc, D.; Dachsel, H.; Deegan, M.; Dyall, K.; Elwood, D.; Glendening, E.; Gutowski, M.; Hess, A.; Jaffe, J.; Johnson, B.; Ju, J.; Kobayashi, R.; Kutteh, R.; Lin, Z.; Littlefield, R.; Long, X.; Meng, B.; Nakajima, T.; Niu, S.; Rosing, M.; Sandrone, G.; Stave, M.; Taylor, H.; Thomas, G.; van Lenthe, J.; Wong, A.; Zhang, Z. *NWChem., A Computational Chemistry Package for Parallel Computers Version 4.7*; Pacific Northwest National Laboratory: Richland, WA, 2005.
(38) Hurley, M. M.; Pacios, L. F.; Christiansen, P. A.; Ross, R. B.; Ermler, W. C. *J. Chem. Phys.* **1986**, *84*, 6840.
(39) LaJohn, L. A.; Christiansen, P. A.; Ross, R. B.; Atashroo, T.; Ermler, W. C. *J. Chem. Phys.* **1987**, *87*, 2812.
(40) (a) King, K. D.; Golden, D. M.; Benson, S. W. *J. Phys. Chem.* **1971**, *75*, 987. (b) Furuyama, S.; Golden, D. M.; Benson, S. W. *J. Am. Chem. Soc.* **1969**, *91*, 7564.
(41) (a) Zheng, X. M.; Kwok, W. M.; Phillips, D. L. *J. Phys. Chem. A* **2000**, *104*, 10464. (b) Zheng, X. M.; Phillips, D. L. *J. Phys. Chem. A* **2000**, *104*, 6880. (c) Zheng, X. M.; Phillips, D. L. *Chem. Phys. Lett.* **2000**, *324*, 175. (d) Zheng, X. M.; Phillips, D. L. *J. Chem. Phys.* **2000**, *113*, 3194.
(42) Simons, J. P.; Tatham, P. E. R. *J. Chem. Soc. A* **1966**, 854.
(43) Mohan, H.; Rao, K. N.; Iyer, R. M. *Radiat. Phys. Chem.* **1984**, *23*, 505.
(44) Maier, G.; Reisenauer, H. P. *Angew. Chem., Int. Ed. Engl.* **1986**, *25*, 819.
(45) Maier, G.; Reisenauer, H. P.; Hu, J.; Schaad, L. J.; Hess, B. A. *J. Am. Chem. Soc.* **1990**, *112*, 5117.
(46) Andrews, L.; Prochaska, F. T.; Ault, B. S. *J. Am. Chem. Soc.* **1979**, *101*, 9.
(47) Mohan, H.; Moorthy, P. N. *J. Chem. Soc., Perkin Trans.* **1990**, *2*, 277.
(48) Audrieth, L. F. *Inorganic Synthesis*; McGraw-Hill Book Co.; New York, 1950; Vol. III, p 38.
(49) Plech, A.; Wulff, M.; Bratos, S.; Mirloup, F.; Vuilleumier, R.; Schotte, F.; Anfinrud, P. A. *Phys. Rev. Lett.* **2004**, *92*, 125505.
(50) Kong, Q. Y.; Wulff, M.; Ihee, H. Manuscript in preparation.
(51) Morino, T.; Nakamura, Y.; Iijima, Y. *J. Chem. Phys.* **1960**, *32*, 643.
(52) Fujitake, M.; Hirota, E. *J. Chem. Phys.* **1989**, *91*, 3426.
(53) Ihee, H.; Lorenc, M.; Kim, T. K.; Kong, Q. Y.; Cammarata, M.; Lee, J. H.; Bratos, S.; Wulff, M. *Science* **2005**, *309*, 1223.
(54) Kong, Q. Y.; Kim, J.; Lorenc, M.; Kim, T. K.; Ihee, H.; Wulff, M. *J. Phys. Chem. A* **2005**, *109*, 10451.
(55) Zhao, C. Y.; Lin, X. F.; Kwok, W. M.; Guan, X. G.; Du, Y.; Wang, D. Q.; Hung, K. F.; Phillips, D. L. *Chem.—Eur. J.* **2005**, *11*, 1093.
(56) Tomioka, H. *Acc. Chem. Res.* **1997**, *30*, 315.
(57) Schwartz, R. L.; Davico, G. E.; Ramond, T. M.; Lineberger, W. C. *J. Phys. Chem. A* **1999**, *103*, 8213.
(58) Barden, C. J.; Schaefer, H. F., III. *J. Chem. Phys.* **2000**, *112*, 6515.
(59) Strand, T. G. *Acta Chem. Scand.* **1967**, *21*, 2111.